PROCEEDINGS OF SCIENCE

ONLINE ICRC 2021
THE ASTROPARTICLE PHYSICS CONFERENCE
Berlin | Germany
37th International Cosmic Ray Conference
12–23 July 2021

Observation of the cosmic ray shadow of the Sun with the ANTARES neutrino telescope

M. Sanguineti[a,b,*] **and A. Romanov**[a,b] **on behalf of the ANTARES Collaboration**
(a complete list of authors can be found at the end of the proceedings)

[a] *Dipartimento di Fisica dell'Università,*
Via Dodecaneso 33, 16146 Genova, Italy
[b] *INFN - Sezione di Genova,*
Via Dodecaneso 33, 16146 Genova, Italy
E-mail: matteo.sanguineti@unige.it, Andrey.Romanov@ge.infn.it

The ANTARES neutrino telescope is operating in the Mediterranean Sea in its full configuration since 2008. On their journey to the Earth, cosmic rays (CRs) can be absorbed by celestial objects, like the Sun, leading to a deficit in atmospheric muons produced by CR interactions from the solid angle region covered by the Sun, the so-called Sun "shadow" effect. This phenomenon can be used to evaluate fundamental telescope characteristics: the detector angular resolution and pointing accuracy. This work describes the study of the Sun "shadow" effect using the ANTARES data collected between 2008 and 2017. The statistical significance of the Sun shadow observation is 3.7σ and the estimated angular resolution value of the ANTARES telescope for downward-going muons is $0.59° \pm 0.10°$. This result is consistent with the expectations obtained from the Monte Carlo simulations and also with the estimation from the Moon "shadow" analysis of 2007-2016 years. No evidence of systematic pointing shift is found and the resulting pointing accuracy is in agreement with the expectations.

37th International Cosmic Ray Conference (ICRC 2021)
July 12th – 23rd, 2021
Online – Berlin, Germany

*Presenter

PoS(ICRC2021)1124

1. Introduction

In its 13 years of operation, the ANTARES neutrino telescope [1] has contributed to multiple searches for neutrinos from point sources, such as blazars, gamma ray bursts or fast radio bursts. Angular resolution and detector pointing are key parameters for this type of study since typically only a small number of signal events are searched for within a consistent background. The spatial correlation of the signals with the known position of the potential source allows the signal-to-background ratio to be drastically reduced. For this reason, a neutrino telescope needs the smallest possible angular resolution and the best possible absolute pointing. This type of detectors cannot use standard candles, such as electromagnetic telescopes, but can exploit the absorption of cosmic rays by celestial objects, such as the Moon or the Sun, to estimate their performance.

In this contribution, we will focus on the measurement of the so-called "Sun shadow" with the ANTARES detector. If cosmic rays on their way to the Earth intercept the Sun, they cannot pass through it. Thus, an observer on the Earth notices a deficit of cosmic rays in the direction of the Sun, so the Sun shadow can be used as a calibration source for a neutrino telescope.

Between 2006 and 2008, the 12 lines of the ANTARES detector were deployed 40 km off the coast of Toulon, France. Each detector line has 25 storeys and each storey houses three 10-inch Photo-Multiplier Tubes (PMTs) inside pressure-resistant glass spheres (the Optical Modules). Each line is 450 m long and the first storey is 100 m above the sea floor. The lines are connected to the shore by an electro-optical cable from the junction box to the shore station.

The neutrino detection mechanism is based on the interaction of neutrinos in the proximity of the detector producing charged particles. These particles have velocities higher than the speed of light in the water, resulting in the emission of Cherenkov light which can be detected by the PMTs of the telescope. By measuring the time and position of the signals (*hits*), the trajectory of the charged particle can be reconstructed (*event*) and thus the direction of origin of the neutrino.

Typically, upward-going events are studied, since downward-going events are dominated by the contribution of atmospheric muons, which is why the PMTs of the detector points downwards at an angle of 45°. However, in this study we will focus on the measurement of downward-going atmospheric muons, as we want to study the effect of the absorption of cosmic rays by the Sun.

The shadow of the Sun or the Moon has already been used by several cosmic ray detectors and the IceCube neutrino telescope to estimate the detector pointing performance [2], while the ANTARES collaboration has already presented a study of the Moon shadow and found a significance of 3.5 σ by analysing a data sample corresponding to a livetime of 3128 days [3].

2. Event selection criteria optimisation

The selection criteria optimisation is based on a Monte Carlo (MC) that features downward-going muon events which are generated with the MUPAGE code. A cylinder (can) surrounding the active volume of the detector, 650 m high, with a radius of 290 m, is considered in the simulation, where muons are generated according to parametric formulas that allow to calculate the flux and the angular distribution of underwater muon bundles [4]. The simulation includes all the steps of the muon detection: propagation of muons in the surroundings of the detector, the emission of Cherenkov light, the light propagation to the PMTs and the digitalisation of the signals [5].

PoS(ICRC2021)1124

The data of the ANTARES telescope are divided into time samples lasting several hours, called *runs*. For each of these runs, the environmental conditions and the detector configuration are recorded, so that the exact data acquisition conditions can be reproduced in the Monte Carlo simulation, the so-called *run-by-run* simulation [6].

The number of atmospheric muons is extremely large, so we typically choose to generate them with a reduced statistic, in our case 1/3. However, in this analysis we can increase the statistic by using the additional zones approach. Instead of focusing only on the region of space where the Sun is at a given instant, one can add additional "artificial suns" by simply shifting the position of the Sun by certain time interval and eliminating the muons generated in these directions, as it is also done in the Monte Carlo for the real position of the Sun. By shifting the position of the Sun by 2 hours, 11 additional zones were obtained, so that the final statistics of our simulation is 4 times larger than in the data.

The optimisation of the selection criteria is performed exploiting two parameters: Λ, the quality of the reconstruction (based on likelihood optimisation of the reconstruction), and β, the angular uncertainty on the reconstructed track direction [7]. In order to exclude the region close to the horizon, where the muon statistic is lower due to muon longer path in Earth atmosphere, tracks with elevation below 15° are excluded.

The hypothesis test approach is used to determine the selection criteria which maximise the sensitivity to the Sun shadow effect. The procedure is based on the production of two MC samples. In the first one no absorption of cosmic rays by the Sun is simulated (hypothesis H_0), while in the other one all muons coming from the direction of the Sun (radius = 0.26°) are eliminated from the simulation (hypothesis H_1), thus simulating the effect of the Sun shadow. The angular distribution of the events is now projected on a histogram as a function of the distance from the Sun centre (histogram bin size=0.4°). Each bin is normalised according to the corresponding area, resulting in an event density.

Assuming that the event population in each bin asymptotically follows a Gaussian probability distribution, two test statistic can be defined for the two different hypotheses (H_0 and H_1)

$$\begin{aligned} \lambda_0 &= \sum_{i=1}^{N_{\text{bins}}} [\frac{(n_0^i - \mu_i)^2}{\sigma_{\mu,i}^2} - \frac{(n_0^i - \nu_i)^2}{\sigma_{\nu,i}^2}], \\ \lambda_1 &= \sum_{i=1}^{N_{\text{bins}}} [\frac{(n_1^i - \mu_i)^2}{\sigma_{\mu,i}^2} - \frac{(n_1^i - \nu_i)^2}{\sigma_{\nu,i}^2}], \end{aligned} \tag{1}$$

with μ_i (ν_i) the expected number of events in the i-th bin under H_1 (H_0) hypothesis, $\sigma_{\mu,i}$ ($\sigma_{\nu,i}$) the error in the i-th bin under H_1 (H_0). The values of n_1 (n_0) are derived according to a Poisson distribution with expectation values equal to μ_i (ν_i). The two test statistic λ_0 and λ_1 corresponds to χ^2 differences.

The two test statistic are computed for 10^6 pseudo-experiments for each set of selection criteria assumed and the one that maximise the sensitivity is selected. For reference, Fig. 1 shows the distribution of the two test statistic λ_0 and λ_1 for the best selection criteria ($\Lambda_{\text{cut}} = -5.9$ and $\beta_{\text{cut}} = 1.1°$).

The significance is computed evaluating the p-value of the λ_0 distribution (null hypothesis, H_0) corresponding to the median of the λ_1 distribution, for which 50% of the pseudo-experiments under

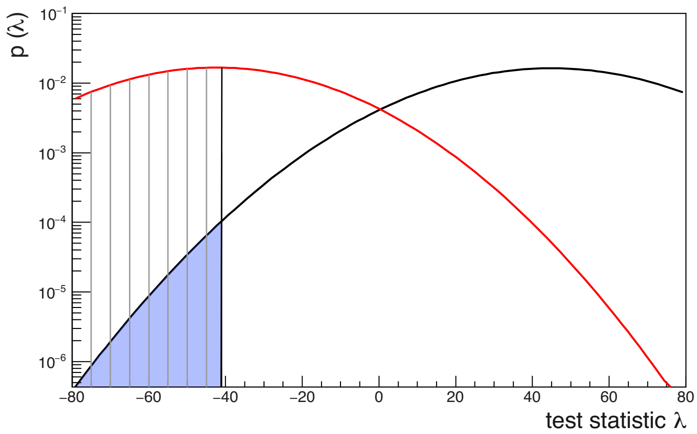

Figure 1: Distribution of the test statistic λ for the two hypotheses, H_0 (black curve) and H_1 (red curve), obtained for the best selection criteria. The dashed area represents the fraction of the distribution (50%) where H_1 hypothesis is correctly identified. The blue area corresponds to the expected median significance (3.4σ) to reject the H_0 hypothesis in favour of the H_1 hypothesis.

the H_1 hypothesis (presence of the Sun shadow) are correctly identified. For the best selection criteria the p-value is equal to 7.4×10^{-4}, corresponding to a significance of 3.4σ. Fig. 2 shows the dependance of the significance on the cuts applied on Λ and β.

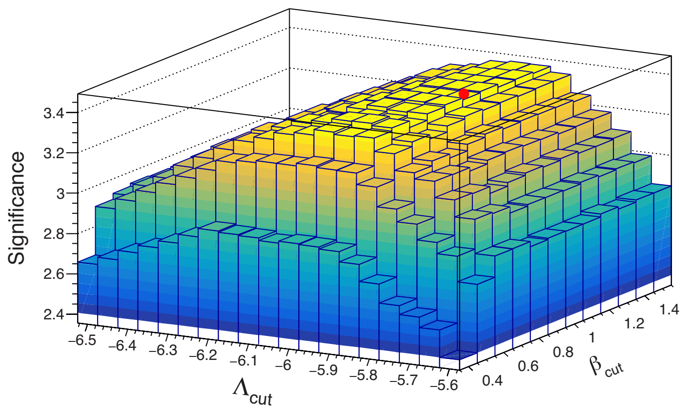

Figure 2: Expected significance of the Sun shadow effect based on pseudo-experiment approach, as a function of cut on Λ and β ($\Lambda_{\rm cut}$ and $\beta_{\rm cut}$). The red point represents the best selection criteria ($\Lambda_{\rm cut} = -5.9$ and $\beta_{\rm cut} = 1.1°$). The expected significance for the selected set of cut values is 3.4σ.

3. Analysis of the 2008-2017 data sample

The ANTARES data sample, corresponding to 2925 days of livetime collected in 10 years (2008-2017), counts 2.6×10^6 events reconstructed as downward-going muons with the standard ANTARES reconstruction chain. After the application of the selection criteria described in the previous section 6.5×10^5 events survived. As previously described, the events are projected on a histogram as a function of the distance from the Sun centre (histogram bin size=0.4°) obtaining Fig. 3.

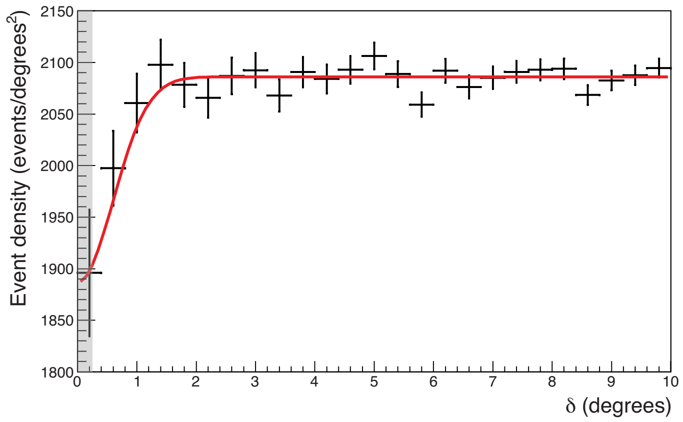

Figure 3: Muon event density as a function of the angular distance δ from the Sun centre (data sample 2008-2017). The red lines represents the histogram fit with Eq. 2. The shaded area corresponds to the Sun radius (0.26°).

The data distribution is fitted with the function

$$f(\delta) = \frac{dN}{d\Omega} = k(1 - \frac{R^2_{\text{Sun}}}{2\sigma^2_{\text{res}}} e^{-\frac{\delta^2}{2\sigma^2_{\text{res}}}}), \tag{2}$$

where Ω is the solid angle of the concentric ring around the Sun centre, k is the average muon event density in the H_0 hypothesis (fitted value $k = 2086 \pm 3$), R_{Sun} is the average angular radius of the Sun (0.26°) and σ_{res} is the width of the Gaussian dip (fitted value $\sigma_{\text{res}} = 0.59° \pm 0.10°$). The number of absorbed events in the Sun shadow dip is $N_{\text{abs}} = k\pi R^2_{\text{Sun}} = 443 \pm 1$.

The influence of the finite-size radius of the Sun in the estimation of the detector resolution is estimated though dedicated pseudo-experiments. The discrepancies obtained between the assumed detector angular resolutions and the fitted values of the Gaussian width are negligible with respect to the statistical uncertainty (below 10% for the assumed angular resolution values above 0.35°) [8].

In the hypothesis of no shadowing effect (H_0), the data distribution in Fig. 3 would follow the profile of Eq. 3,

$$\frac{dN}{d\Omega} = k; \tag{3}$$

the Sun shadow significance can be estimated fitting the event density according the two different hypotheses defining the test statistic $-\lambda = \chi^2_0 - \chi^2_1$. For the 2008-2017 sample the significance of the shadowing effect is 3.7σ. Unfortunately the data sample is not sufficient to study how the significance depends on the activity of the Sun.

The measurement of the Sun shadow allows also an estimation of the detector pointing performance. For this purpose the data sample is projected on a 2D-histogram as a function of $x = (\alpha_\mu - \alpha_{\text{Sun}}) \times \cos(h_\mu)$ and $y = h_\mu - h_{\text{Sun}}$, where α_μ, α_{Sun} are the azimuthal coordinates and h_μ, h_{Sun} are the elevation angles of the reconstructed track and the Sun, respectively. The bin size is $0.4° \times 0.4°$ spanning the range $[-10°, 10°]$.

First, in the H_0 hypothesis (no shadowing effect), the background distribution is assumed as

$$p_2(x, y; \mathbf{k}) = k_0 + k_1 x + k_2 x^2 + k_3 y + k_4 y^2, \tag{4}$$

while, in the H_1 hypothesis (presence of the shadowing effect), the data distribution is approximated with a function obtained by subtracting from $p_2(x, y; \mathbf{k})$ a two-dimensional Gaussian function:

$$G(x, y; A_{sh}, x_s, y_s) = \frac{A_{sh}}{2\pi\sigma_{\text{res}}^2} e^{-\frac{(x-x_s)^2+(y-y_s)^2}{2\sigma_{\text{res}}^2}}, \tag{5}$$

where A_{sh} is the amplitude of the deficit caused by the shadowing effect (free parameter), (x_s, y_s) is the assumed position of the Sun. The width of the Gaussian function is assumed equal in both x and y direction ($\sigma_{\text{res}} = 0.59°$).

The procedure applied foresees the assumption of different Sun shadow centre positions spanning the whole region of interest with a step size of 0.1°. The nominal Sun position is $O \equiv (0°, 0°)$. Then the test statistic $\lambda(x_s, y_s)$ is computed as

$$\lambda(x_s, y_s) = \chi^2_{H_1}(x_s, y_s) - \chi^2_{H_0}, \tag{6}$$

where $\chi^2_{H_0}$ is the χ^2 value obtained from the fit with Eq. 4, which is a constant value for all the bins of the histogram, and $\chi^2_{H_1}(x_s, y_s)$ is the χ^2 value obtained from the fit with the function used to describe hypothesis H_1, $p_2(x, y; \mathbf{k}) - G(x, y; A_{sh}, x_s, y_s)$.

The result is provided in Fig. 4 where the values of the test statistic $\lambda(x_s, y_s)$ as a function of the assumed Sun position is shown. The minimum value is $\lambda_{\text{min}} = -13.7$ in the position $\lambda(x_s, y_s) = (0.2°, 0°)$. The values of $\lambda(x_s, y_s)$ and A_{sh} for the nominal Sun position are $\lambda_O = -13.1$ and $A_O = 54 \pm 15$. As the $-\lambda$ follows the distribution of a χ^2 with one degree of freedom, the significance to reject the no-Sun hypothesis can be computed (p-value= 3.1×10^{-4}, significance=3.6σ)

The test statistic $\lambda(x_s, y_s)$ behaves as a bi-dimensional profile-likelihood, with A_{sh} treated as the nuisance parameter and the interval corresponding to a desired confidence level (CL) is obtained for $\lambda(x_s, y_s) \leq \lambda_{\text{cut}} = \lambda_{\text{min}} + Q$, where Q is the quantile for the joint estimation of two parameters (Fig. 5).

4. Conclusions

This contribution presented the study of the Sun shadowing effect in 2008-2017 ANTARES data sample (2925 days of livetime).

The two strategies applied in this analysis achieved compatible results showing a significance of the phenomenon equal to 3.7σ using the one-dimensional approach. Besides the ANTARES detector is designed to maximise the angular resolution for upward-going track (PMTs are pointing 45°

PoS(ICRC2021)1124

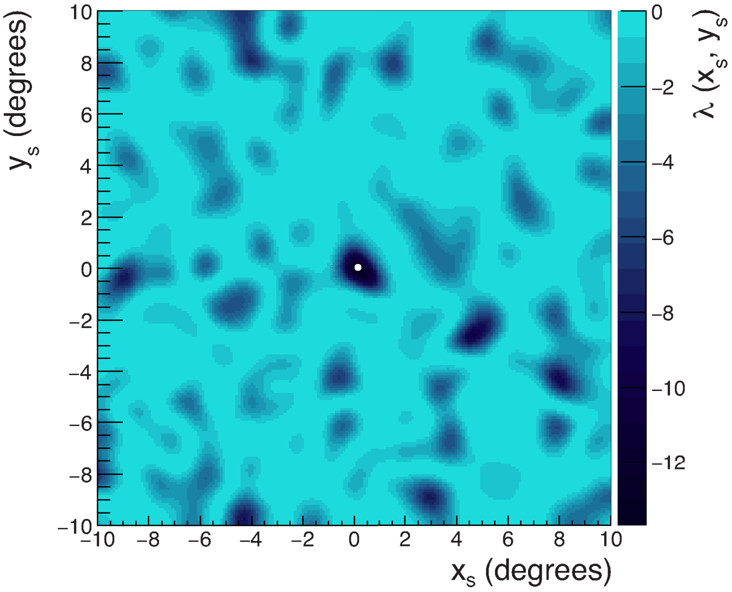

Figure 4: The distribution of the test statistic $\lambda(x_s, y_s)$. The minimum value $\lambda_{\text{min}} = -13.7$ is found at $(0.2°, 0°)$ point (white dot).

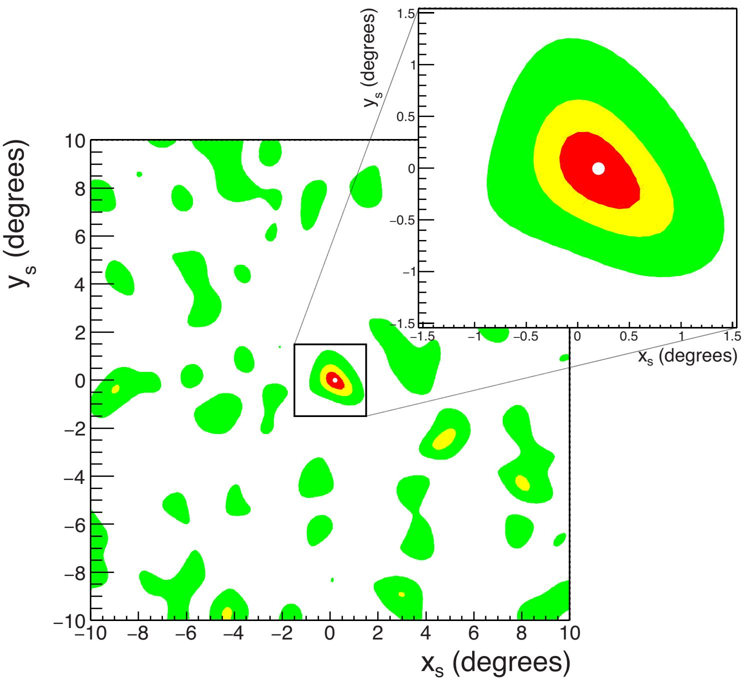

Figure 5: Contours corresponding to different confidence levels (red: 68.27%; yellow: 95.45%; green: 99.73%). The white dot indicates $(0.2°, 0°)$ point for which a minimum value of $\lambda_{\text{min}} = -13.7$ is obtained.

below the horizon), this study demonstrated that the ANTARES angular resolution for downward-going muons is $0.59° \pm 0.10°$. This results is compatible with the previous Moon shadow analysis ($0.73° \pm 0.14°$) [3].

The pointing performance study did not evidence any significant deviation from the expectations, confirming the results of the Moon shadow study [3].

References

[1] Ageron, M. and others. *ANTARES: the first undersea neutrino telescope*. Nucl. Instrum. Meth. A, 656, 11-38 (2011)

[2] Aartsen, M. G. and others. *Detection of the Temporal Variation of the Sun's Cosmic Ray Shadow with the IceCube Detector*. Astrophys. J., 872, 2, 133 (2019)

[3] Albert, A. and others. *The cosmic ray shadow of the Moon observed with the ANTARES neutrino telescope*. Eur. Phys. J. C, 78, 12, 1006 (2018)

[4] Carminati, G. and others. *Atmospheric MUons from PArametric formulas: a fast GEnerator for neutrino telescopes (MUPAGE)*. Computer Physics Communications, 179, 12, 915-923 (2008)

[5] Aguilar, J.A. and others. *The data acquisition system for the ANTARES neutrino telescope*. Nucl. Instrum. Meth. A, 570, 107-116 (2007)

[6] Albert, A. and others. *Monte Carlo simulations in the ANTARES underwater neutrino telescope* . JCAP01, 064 (2021)

[7] Adrian-Martinez, S. and others. *First search for neutrinos in correlation with gamma-ray bursts with the ANTARES neutrino telescope*. JCAP, 03, 006 (2013)

[8] Albert, A. and others. *Observation of the cosmic ray shadow of the Sun with the ANTARES neutrino telescope*. Phys. Rev. D, 102, 12, 122007 (2020)

PoS(ICRC2021)1124

Full Authors List: ANTARES Collaboration

A. Albert[1,2], S. Alves[3], M. André[4], M. Anghinolfi[5], G. Anton[6], M. Ardid[7], S. Ardid[7], J.-J. Aubert[8], J. Aublin[9], B. Baret[9], S. Basa[10], B. Belhorma[11], M. Bendahman[9,12], V. Bertin[8], S. Biagi[13], M. Bissinger[6], J. Boumaaza[12], M. Bouta[14], M.C. Bouwhuis[15], H. Brânzaş[16], R. Bruijn[15,17], J. Brunner[8], J. Busto[8], B. Caiffi[5], A. Capone[18,19], L. Caramete[16], J. Carr[8], V. Carretero[3], S. Celli[18,19], M. Chabab[20], T. N. Chau[9], R. Cherkaoui El Moursli[12], T. Chiarusi[21], M. Circella[22], A. Coleiro[9], M. Colomer-Molla[9,3], R. Coniglione[13], P. Coyle[8], A. Creusot[9], A. F. Díaz[23], G. de Wasseige[9], A. Deschamps[24], C. Distefano[13], I. Di Palma[18,19], A. Domi[15,17], C. Donzaud[9,25], D. Dornic[8], D. Drouhin[1,2], T. Eberl[6], T. van Eeden[15], D. van Eijk[15], N. El Khayati[12], A. Enzenhöfer[8], P. Fermani[18,19], G. Ferrara[13], F. Filippini[21,26], L.A. Fusco[8], Y. Gatelet[9], P. Gay[27,9], H. Glotin[28], R. Gozzini[3], R. Gracia Ruiz[15], K. Graf[6], C. Guidi[5,29], S. Hallmann[6], H. van Haren[30], A.J. Heijboer[15], Y. Hello[24], J.J. Hernández-Rey[3], J. Hößl[6], J. Hofestädt[6], F. Huang[8], G. Illuminati[9,21,26], C.W James[31], B. Jisse-Jung[15], M. de Jong[15,32], P. de Jong[15], M. Kadler[33], O. Kalekin[6], U. Katz[6], N.R. Khan-Chowdhury[3], A. Kouchner[9], I. Kreykenbohm[34], V. Kulikovskiy[5,36], R. Lahmann[6], R. Le Breton[9], D. Lefèvre[35], E. Leonora[36], G. Levi[21,26], M. Lincetto[8], D. Lopez-Coto[37], S. Loucatos[38,9], L. Maderer[9], J. Manczak[3], M. Marcelin[10], A. Margiotta[21,26], A. Marinelli[39], J.A. Martínez-Mora[7], K. Melis[15,17], P. Migliozzi[39], A. Moussa[14], R. Muller[15], L. Nauta[15], S. Navas[37], E. Nezri[10], B. O'Fearraigh[15], A. Păun[16], G.E. Păvălaş[16], C. Pellegrino[21,40,41], M. Perrin-Terrin[8], V. Pestel[15], P. Piattelli[13], C. Pieterse[3], C. Poirè[7], V. Popa[16], T. Pradier[1], N. Randazzo[36], S. Reck[6], G. Riccobene[13], A. Romanov[5,29], A. Sánchez-Losa[3,22], F. Salesa Greus[3], D. F. E. Samtleben[15,32], M. Sanguineti[5,29], P. Sapienza[13], J. Schnabel[6], J. Schumann[6], F. Schüssler[38], M. Spurio[21,26], Th. Stolarczyk[38], M. Taiuti[5,29], Y. Tayalati[12], S.J. Tingay[31], B. Vallage[38,9], V. Van Elewyck[9,41], F. Versari[21,26,9], S. Viola[13], D. Vivolo[39,43], J. Wilms[34], S. Zavatarelli[5], A. Zegarelli[18,19], J.D. Zornoza[3], and J. Zúñiga[3]

[1]Université de Strasbourg, CNRS, IPHC UMR 7178, F-67000 Strasbourg, France.
[2]Université de Haute Alsace, F-68100 Mulhouse, France.
[3]IFIC - Instituto de Física Corpuscular (CSIC - Universitat de València) c/ Catedrático José Beltrán, 2 E-46980 Paterna, Valencia, Spain.
[4]Technical University of Catalonia, Laboratory of Applied Bioacoustics, Rambla Exposició, 08800 Vilanova i la Geltrú, Barcelona, Spain.
[5]INFN - Sezione di Genova, Via Dodecaneso 33, 16146 Genova, Italy.
[6]Friedrich-Alexander-Universität Erlangen-Nürnberg, Erlangen Centre for Astroparticle Physics, Erwin-Rommel-Str. 1, 91058 Erlangen, Germany.
[7]Institut d'Investigació per a la Gestió Integrada de les Zones Costaneres (IGIC) - Universitat Politècnica de València. C/ Paranimf 1, 46730 Gandia, Spain.
[8]Aix Marseille Univ, CNRS/IN2P3, CPPM, Marseille, France.
[9]Université de Paris, CNRS, Astroparticule et Cosmologie, F-75013 Paris, France.
[10]Aix Marseille Univ, CNRS, CNES, LAM, Marseille, France.
[11]National Center for Energy Sciences and Nuclear Techniques, B.P.1382, R. P.10001 Rabat, Morocco.
[12]University Mohammed V in Rabat, Faculty of Sciences, 4 av. Ibn Battouta, B.P. 1014, R.P. 10000 Rabat, Morocco.
[13]INFN - Laboratori Nazionali del Sud (LNS), Via S. Sofia 62, 95123 Catania, Italy.
[14]University Mohammed I, Laboratory of Physics of Matter and Radiations, B.P.717, Oujda 6000, Morocco.
[15]Nikhef, Science Park, Amsterdam, The Netherlands.
[16]Institute of Space Science, RO-077125 Bucharest, Măgurele, Romania.
[17]Universiteit van Amsterdam, Instituut voor Hoge-Energie Fysica, Science Park 105, 1098 XG Amsterdam, The Netherlands.
[18]INFN - Sezione di Roma, P.le Aldo Moro 2, 00185 Roma, Italy.
[19]Dipartimento di Fisica dell'Università La Sapienza, P.le Aldo Moro 2, 00185 Roma, Italy.
[20]LPHEA, Faculty of Science - Semlali, Cadi Ayyad University, P.O.B. 2390, Marrakech, Morocco.
[21]INFN - Sezione di Bologna, Viale Berti-Pichat 6/2, 40127 Bologna, Italy.
[22]INFN - Sezione di Bari, Via E. Orabona 4, 70126 Bari, Italy.
[23]Department of Computer Architecture and Technology/CITIC, University of Granada, 18071 Granada, Spain.
[24]Géoazur, UCA, CNRS, IRD, Observatoire de la Côte d'Azur, Sophia Antipolis, France.
[25]Université Paris-Sud, 91405 Orsay Cedex, France.
[26]Dipartimento di Fisica e Astronomia dell'Università, Viale Berti Pichat 6/2, 40127 Bologna, Italy.
[27]Laboratoire de Physique Corpusculaire, Clermont Université, Université Blaise Pascal, CNRS/IN2P3, BP 10448, F-63000 Clermont-Ferrand, France.
[28]LIS, UMR Université de Toulon, Aix Marseille Université, CNRS, 83041 Toulon, France.
[29]Dipartimento di Fisica dell'Università, Via Dodecaneso 33, 16146 Genova, Italy.
[30]Royal Netherlands Institute for Sea Research (NIOZ), Landsdiep 4, 1797 SZ 't Horntje (Texel), the Netherlands.
[31]International Centre for Radio Astronomy Research - Curtin University, Bentley, WA 6102, Australia.
[32]Huygens-Kamerlingh Onnes Laboratorium, Universiteit Leiden, The Netherlands.
[33]Institut für Theoretische Physik und Astrophysik, Universität Würzburg, Emil-Fischer Str. 31, 97074 Würzburg, Germany.
[34]Dr. Remeis-Sternwarte and ECAP, Friedrich-Alexander-Universität Erlangen-Nürnberg, Sternwartstr. 7, 96049 Bamberg, Germany.
[35]Mediterranean Institute of Oceanography (MIO), Aix-Marseille University, 13288, Marseille, Cedex 9, France; Université du Sud Toulon-Var, CNRS-INSU/IRD UM 110, 83957, La Garde Cedex, France.
[36]INFN - Sezione di Catania, Via S. Sofia 64, 95123 Catania, Italy.

[37]Dpto. de Física Teórica y del Cosmos & C.A.F.P.E., University of Granada, 18071 Granada, Spain.
[38]IRFU, CEA, Université Paris-Saclay, F-91191 Gif-sur-Yvette, France.
[39]INFN - Sezione di Napoli, Via Cintia 80126 Napoli, Italy.
[40]Museo Storico della Fisica e Centro Studi e Ricerche Enrico Fermi, Piazza del Viminale 1, 00184, Roma.
[41]INFN - CNAF, Viale C. Berti Pichat 6/2, 40127, Bologna.
[42]Institut Universitaire de France, 75005 Paris, France.
[43]Dipartimento di Fisica dell'Università Federico II di Napoli, Via Cintia 80126, Napoli, Italy.